PUBLISHED VERSION

Stevenson, Mark Andrew; Hargreaves, Leigh Randall; Lohmann, Birgit; Bray, Igor; Fursa, D. V.; Bartschat, K.; Kheifets, A.
Fully differential cross-section measurements for electron-impact ionization of neon and xenon Physical Review A, 2009; 79(1):012709

© 2009 American Physical Society

http://link.aps.org/doi/10.1103/PhysRevA.79.012709

PERMISSIONS

http://publish.aps.org/authors/transfer-of-copyright-agreement

"The author(s), and in the case of a Work Made For Hire, as defined in the U.S. Copyright Act, 17 U.S.C.

§101, the employer named [below], shall have the following rights (the "Author Rights"):

[...]

3. The right to use all or part of the Article, including the APS-prepared version without revision or modification, on the author(s)' web home page or employer's website and to make copies of all or part of the Article, including the APS-prepared version without revision or modification, for the author(s)' and/or the employer's use for educational or research purposes."

19th March 2013

http://hdl.handle.net/2440/52054

Fully differential cross-section measurements for electron-impact ionization of neon and xenon

M. A. Stevenson,[1] L. R. Hargreaves,[1] B. Lohmann,[1] I. Bray,[2] D. V. Fursa,[2] K. Bartschat,[3] and A. Kheifets[4]
[1]*ARC Centre of Excellence for Antimatter-Matter Studies, The University of Adelaide, Adelaide, South Australia 5005, Australia*
[2]*ARC Centre of Excellence for Antimatter-Matter Studies, Curtin University, Perth, Western Australia, Australia*
[3]*Department of Physics and Astronomy, Drake University, Des Moines, Iowa 50311, USA*
[4]*Research School of Physical Sciences, Australian National University, Canberra, Australian Capital Territory, Australia*
(Received 26 October 2008; published 22 January 2009)

We present a combined experimental and theoretical investigation of the fully differential cross section for electron-impact ionization of neon and xenon. The experiments were performed under coplanar asymmetric kinematics, at intermediate incident electron energies, and for a range of scattered electron detection angles. The experimental results are compared with three calculations: a convergent close-coupling calculation, a distorted-wave Born approximation (DWBA) calculation with inclusion of the Gamow factor, and a hybrid DWBA+R-matrix calculation. The comparison between the experimental and theoretical results highlights the importance of the description of postcollision interaction, and the results exhibit interesting orbital-dependent differences.

DOI: 10.1103/PhysRevA.79.012709 PACS number(s): 34.80.Dp

INTRODUCTION

In recent years there has been dramatic progress in the theoretical description of the electron-impact ionization process, as evidenced by the ability of modern calculations to, in many cases, correctly describe the cross section (often called the triple differential cross section) which is obtained from kinematically complete measurements of the process—experiments in which the linear momenta of the incoming and two outgoing electrons are fully determined. Indeed, the electron impact ionization of atomic hydrogen is now considered to be a solved problem [1,2], and enormous progress has been made in describing ionization of the two-electron helium target [3,4]. The ultimate aim of these investigations is to provide a "complete" scattering theory; one that can describe any ionization process, over all possible energies, for any degree of target complexity. As such, the focus of research is now shifting toward understanding ionization of heavier targets. For larger atoms, good progress has been made in describing (and explaining) the form of the triple differential cross section (TDCS), but there are certain kinematic regimes where significant problems still exist. The variability in the predictive power of modern calculations is illustrated by recent measurements of the TDCS for ionization of the $3s$ and $3p$ orbitals of argon at intermediate incident electron energies (of the order of five times the binding energy) [5–7], and further measurements of the TDCS for ionization of the $2s$ and $2p$ orbitals of neon [8], the latter being performed at considerably higher incident energies (600 eV) and in a kinematic regime corresponding to large energy transfer in the process. Significant discrepancies were observed between state-of-the-art theoretical calculations and the experimental results for the case of argon $3p$ and $3s$ ionization at intermediate energies; in particular, there was a marked difference in the level of agreement for ionization of different orbitals. In contrast, at higher incident energies, very good agreement was observed between theory and experiment, even across a comparison of three different theoretical calculations and two different sets of experiments. Similarly good agreement has been noted in a recent paper examining in more detail the TDCS for ionization of neon and argon at the higher incident energy of 600 eV [9].

These studies suggest that a major challenge still exists for theoretical calculations of the electron impact ionization process in the intermediate energy regime. In this paper we present a joint experimental and theoretical investigation of the TDCS for electron impact ionization of the neon $2s$ and $2p$ orbitals, and the xenon $5p_{3/2}$ orbital. The relatively large fine-structure splitting of the outer $5p_{3/2}$ and $5p_{1/2}$ suborbitals (1.3 eV) is readily resolvable. The measurements were performed at an incident electron energy of 150 eV, an ejected electron energy of 10 eV, and emission angles for the fast scattered electron of −15°, −10°, and −5°. The scattered electron energy is determined by the energy conservation condition

$$E_0 = E_a + E_b + \varepsilon_i,$$

where E_0 is the incident electron energy (with momentum $\mathbf{k}_0$), E_a and E_b are the scattered and ejected electron energies (with scattering and ejection angles of θ_a and θ_b and momenta $\mathbf{k}_a$ and $\mathbf{k}_b$), respectively, and ε_i is the ionization potential of the ionized orbital [helium=24.6 eV, neon $(2p)$ =21.6 eV, $(2s)$=47.7 eV, xenon $(5p_{3/2})$=12.1 eV]. The momentum transferred during the collision is given by $\mathbf{K}=\mathbf{k}_0 - \mathbf{k}_a$. Varying the scattered electron angle while keeping the other kinematical parameters constant is equivalent to varying the momentum transferred to the target during the collision.

EXPERIMENT

The $(e,2e)$ spectrometer used in these experiments has been described in detail in a previous publication [5]; hence, only a brief description is given here. A collimated, monoenergetic electron beam is produced from an electron gun comprised of six cylindrical-cross-section lens elements, with a heated tungsten filament as the electron source. The resultant beam has an energy spread of approximately 0.5 eV full

 ©2009 The American Physical Society

width at half maximum (FWHM) and a beam diameter of 1 mm. This crosses a target gas jet produced from a stainless steel capillary of 0.7 mm diameter; the interaction region is formed by the intersection of the gas jet and the electron beam. Two identical hemispherical electron energy analyzers collect the outgoing electrons from the interaction region. The analyzers are mounted on independently rotatable turntables, driven by stepper motors. Using a four-element input lens system, electrons emerging from ionization events are decelerated, focused into, and passed through the analyzers' energy-selective hemispherical lens section before being detected by channel electron multipliers. The signals are then analyzed using standard fast timing electronics and coincidence circuitry, with an overall energy resolution in coincidence mode of around 0.75 eV FWHM. During measurements for the chosen geometry, the scattered electron is detected at a small fixed angle while the in-plane angular distribution of ejected electrons is measured by rotating the ejected electron analyzer around the scattering plane. The scattered electron angle is designated as a negative angle, since it is in the opposite half of the scattering plane from the forward directed part of the ejected electron distribution. The measurements and data analysis are performed under computer control, where the ejected electron energy analyzer is scanned repeatedly over the desired angular range to reduce random fluctuations in the data.

The angular coverage of conventional $(e,2e)$ spectrometers is normally restricted due to the relative positions of the electron gun and analyzers; for our apparatus this typically limits measurements of the ejected electron angular distribution to between 45°–135° and 225°–285° for the chosen geometry and kinematics. To overcome this, the angular range has been extended by incorporating a magnetic angle-changing device (MAC) [10] into the spectrometer. The use of this technique in an $(e,2e)$ spectrometer has also been described in detail elsewhere [11,12]. Briefly, a localized magnetic field is introduced to the interaction region using a system of solenoids. This field, perpendicular to the scattering plane, deflects the incident, scattered and ejected electrons in the scattering plane. Using a combination of inner and outer solenoids with appropriate magnetic field configurations ensures that (i) the incident beam always passes through the interaction region, and (ii) the scattered and ejected electrons always exit the deflecting field in a radial direction. Due to the asymmetric energy sharing, the slow ejected electron undergoes a much greater deflection than the faster incident and scattered electrons. The resultant total deflection (made up of the incident and ejected electron deflections, $\Delta\theta_{\mathrm{inc}}+\Delta\theta_b$) moves the ejected electrons from inaccessible to accessible regions. This allows us to cover an extended, and for certain kinematics, complete coplanar angular range [12].

THEORY

Distorted-wave Born approximation+*R*-matrix approach

The hybrid distorted-wave Born approximation (DWBA)+*R*-matrix computational approach is based upon the formalism outlined by Bartschat and Burke [13] and the computer program RMATRX-ION of Bartschat [14]. The basic idea is to describe a "fast" projectile electron by a distorted wave and then calculate the initial bound state and the interaction between the residual ion and a "slow" ejected electron by an *R*-matrix (close-coupling) expansion. Second-order effects in the projectile-target interaction were accounted for approximately, as outlined by Reid *et al.* [15]. Results from this second-order distorted-wave (DW2) plus *R*-matrix (RM) hybrid method will be labeled DW2-RM below.

For both the neon and xenon targets, we used a distorted-wave representation for the projectile, with the distorted waves calculated in the static potential of the initial state, and a two-state close-coupling approximation for electron scattering from the residual ion, coupling the ionic ground state $(2s^22p^5)^2P^o$ and the first excited state $(2s2p^2)^2S$ for neon and the corresponding $(5s^25p^5)^2P^o$ and $(5s5p^6)^2S$ states for xenon, respectively. The ionic target description for neon is the one used first by Burke and Taylor [16] for the corresponding photoionization problem. For xenon, a similar multiconfiguration expansion was generated, allowing for single and double promotion of the outer-shell electrons into specially designed pseudo-orbitals 6*s*, 6*p*, and 5*d*. Employing the latter pseudo-orbitals significantly improved the description of the initial bound state, the theoretical energy splitting between the two ionic states, and the results for the oscillator strengths.

In this hybrid method, exchange between the ejected electron and the residual target ion is treated in a computationally exact way, since the close-coupling expansion for this part of the problem is based on fully antisymmetrized wave functions. Also, some channel-coupling effects are included, and it is possible to calculate ionization cross sections for the final ionic states (here $^2P^o$ and ^2S) within the same model individually. On the other hand, exchange between the projectile and the target is neglected, as are any post-collision effects between the two final-state electrons. In principle, this can be done in the same way as in the DWBA-Gamow model described below, and one expects similar qualitative changes of the final results (see below).

Finally, partial waves up to orbital angular momenta of $l=90$ for the fast projectile guaranteed the convergence of its partial wave expansion. Furthermore, the Coulomb interaction between the fast projectile and the target was accounted for through the multipole components $\lambda=0-6$. This range of multipole components proved to be sufficient for the present cases of interest.

DWBA-Gamow model

The distorted-wave Born approximation corrected for the postcollision interaction (PCI) by the phenomenological Gamow (G) factor is described in detail in [9]. In brief, within this model, the projectile-target interaction is treated perturbatively to the lowest order (the so-called first Born approximation). In contrast, the effect of the target potential on the projectile and the two outgoing electrons and their exchange with the core electrons is included fully within the frozen-core Hartree-Fock numerical scheme [17]. The long-range Coulomb interaction in the final state (PCI) is ac-

counted for by introducing the phenomenological Gamow factor that represents the spherically averaged Coulomb density of states [18].

This model was validated in comparison with a large body of experimental data on $(e,2e)$ reactions on helium $(1s^2)$, neon $(2s^2)$, neon $(2p^6)$, and argon $(3p^6)$ under kinematics characterized by large energy transfer and close to minimum momentum transfer from the projectile to the target [8,9]. A good agreement between theory and experiment was found in all cases when the shape of the angular distribution of the two outgoing electrons was analyzed. Information about the magnitude of the cross section is lost in this model since the Gamow factor violates the normalization of the two-electron continuum. In terms of the partial wave expansion, the calculation was fully converged with $l=40$ for the fast projectile and $l=8$ for the slow ejected electron.

Convergent close-coupling approach

The convergent close-coupling (CCC) method treats ionization on the same footing as excitation [2,3]. The total electron-atom wave function is expanded using a complete set of square-integrable states, and solving the resultant close-coupling equations yields scattering amplitudes for all open states. Ionization is associated with excitation of the positive-energy, relative to the residual ion, states. The method has been implemented for targets that can be reasonably treated as one or two valence electrons above an inert core. Consequently it has been very successful in treating the atomic hydrogen [2] and helium [3,4] targets and should be valid for all geometries and kinematics of interest. When it comes to targets such as neon, however, the method has very limited application. We have to suppose that the six $2p$ electrons are part of the inert core and that only the two $2s$ electrons are excitable during the collision. This, rather severe, approximation is best at the higher energies where the Born approximation is dominant. Furthermore, such a treatment yields results only for the ejection of a $2s$ electron, and is unable to yield results for the case where a $2p$ electron is ejected.

Presently the e-Ne CCC calculations were performed using a total of 265 states in the expansion of the total wave function. These comprised 24 S, 23 P, 23 D, 22 F, 21 G and 20 H states, of both singlet and triplet (one less S-triplet state) symmetry. These were sufficient for convergence for the case of interest. They were constructed assuming that the inner $2s$ electron remains in the ground state of the neon ion. The projectile electron was treated with orbital angular momenta extending to 30 partial waves. Exchange between the projectile and the target core and valence electrons was fully included.

RESULTS AND DISCUSSION

The experimental and theoretical results are presented in Figs. 1–6. The measured cross sections are on a relative scale; absolute values are not determined. However, the relative cross sections measured for a given target and orbital at different scattered electron angles have been internormalized. This was achieved by fixing the ejected electron detection angle, and then measuring the coincidence counts alternately between different scattering angles for a fixed time. In all plots, the error bars are statistical and represent one standard deviation. There is an additional uncertainty in the ratio of the binary to recoil peak of no more than 16% for neon $2p$ ionization, 34% for neon $2s$ ionization, and 7% for xenon $5p$ ionization. There is also an uncertainty associated with the internormalization measurements of no more than 8% for xenon and neon $(2p)$, and no more than 18% for neon $(2s)$.

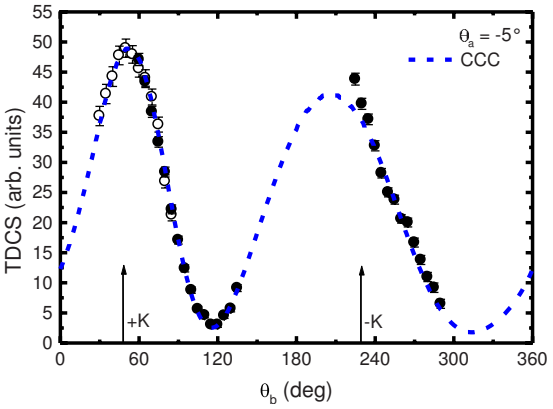

FIG. 1. (Color online) Measured and calculated triple differential cross sections for electron-impact ionization of the $1s$ orbital of helium, under kinematic conditions of $E_0=150$ eV and $E_b=10$ eV. Experimental results with the MAC turned on (open circles) and off (full circles) are shown.

In these experiments, we have used the MAC to extend the lower angular limit in the binary region (enabling us to mostly or fully resolve the binary peak) and the upper angular limit in the recoil region. For measurements performed using the MAC, the deflection is chosen so that a significant portion of the angular range overlaps with the adjoining angular region measured without the MAC. The MAC data are then normalized to the data without the MAC by a visual fit of the two data sets in the overlapping region. The data sets measured using the MAC contain an estimated angular uncertainty of around $+/-5°$.

To check the reliability of the "$(e,2e)$ with MAC" technique, we performed test measurements on helium under identical kinematics to those used in the investigations of neon and xenon, at a scattering angle of 5°; only the scattered electron energy was adjusted to account for the different ionization potential of helium. We then compared the helium measurement with a CCC calculation that is believed to be a benchmark calculation for helium over this energy range [19]. An example of such a test run is shown in Fig. 1, where the ejected electrons in the binary region have been deflected by 50° using the MAC. Here, the experimental data is normalized to the theory at the binary peak maximum. The agreement between experiment and theory in the binary region, for both "MAC-on" and "MAC-off" data, is very good, and such cross sections were recorded at intervals as required during measurements, after which the gas target was changed to the target under investigation and the scattered energy was readjusted.

The results for ionization of the $2s$ orbital of neon are presented in Fig. 2. The momentum transferred during the

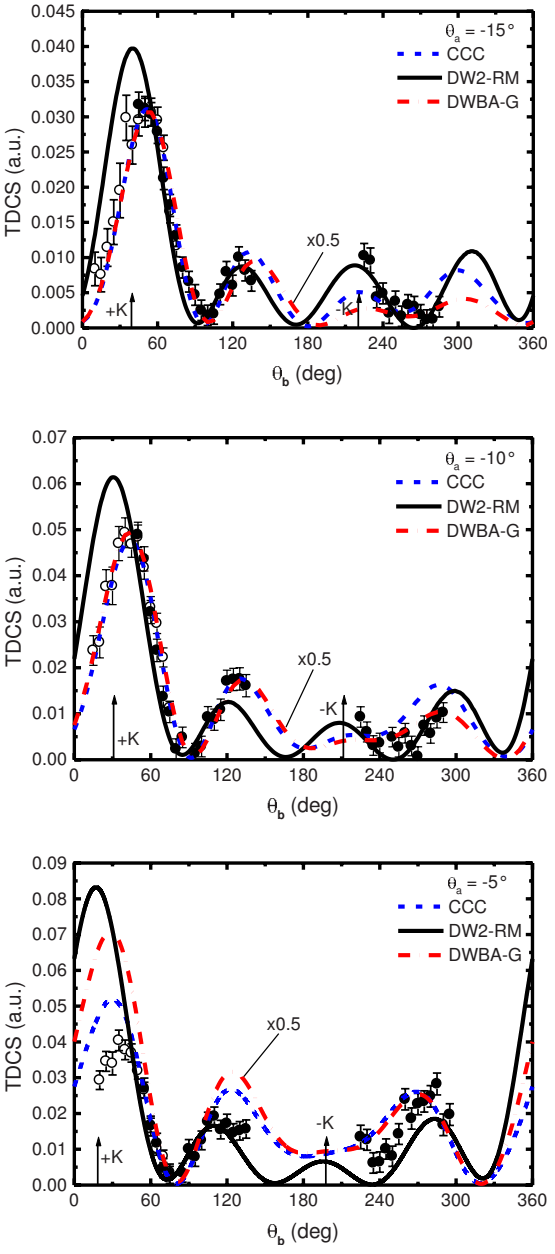

FIG. 2. (Color online) Measured and calculated triple differential cross sections for electron-impact ionization of the 2*s* orbital of neon, under kinematic conditions of $E_0=150$ eV and $E_b=10$ eV. Experimental results with the MAC turned on (open circles) and off (full circles) are shown, with the experimental data normalized to the CCC calculation at $\theta_a=-15°$.

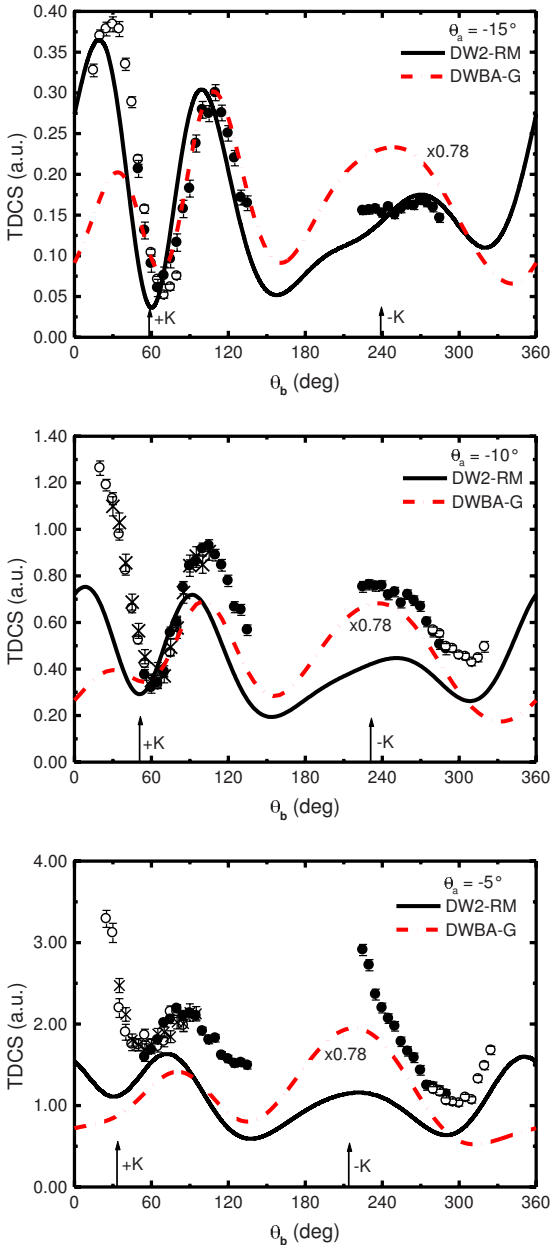

FIG. 3. (Color online) Measured and calculated triple differential cross sections for electron-impact ionization of the 2*p* orbital of neon, under kinematic conditions of $E_0=150$ eV and $E_b=10$ eV. Experimental results with the MAC turned on (open circles and crosses, corresponding to different deflections) and off (full circles) are shown, with the experimental data normalized to the DW2-RM calculation at $\theta_a=-15°$.

collision for scattering angles of $\theta_a=-15°$, $-10°$, and $-5°$ is 1.04, 0.88, and 0.76 a.u., respectively. As the 10 eV ejected electron carries away 0.87 a.u. of momentum, all three scattering angles correspond to kinematic conditions on or near the Bethe ridge [20], where the ion is essentially a spectator during the collision.

Both the experimental and theoretical cross sections indicate a double-peak structure in both the binary and the recoil regions. The experimental data at a scattering angle of $-15°$ have been normalized at the first peak in the binary region to the CCC calculation. The experimental results at scattering angles of $-10°$ and $-5°$ are internormalized to the data at $-15°$ using the experimentally determined ratios. It is noteworthy that the three calculations predict different magnitudes for the cross section; in order to display all three theoretical calculations on the same graph, the DWBA-G results have been multiplied by a constant factor of 0.5, thereby yielding DWBA-G cross sections with the same magnitude as the CCC at the binary peak of the $\theta_a=-15°$ data.

In general, the agreement between the three theoretical calculations and the experimental data is good, in terms of

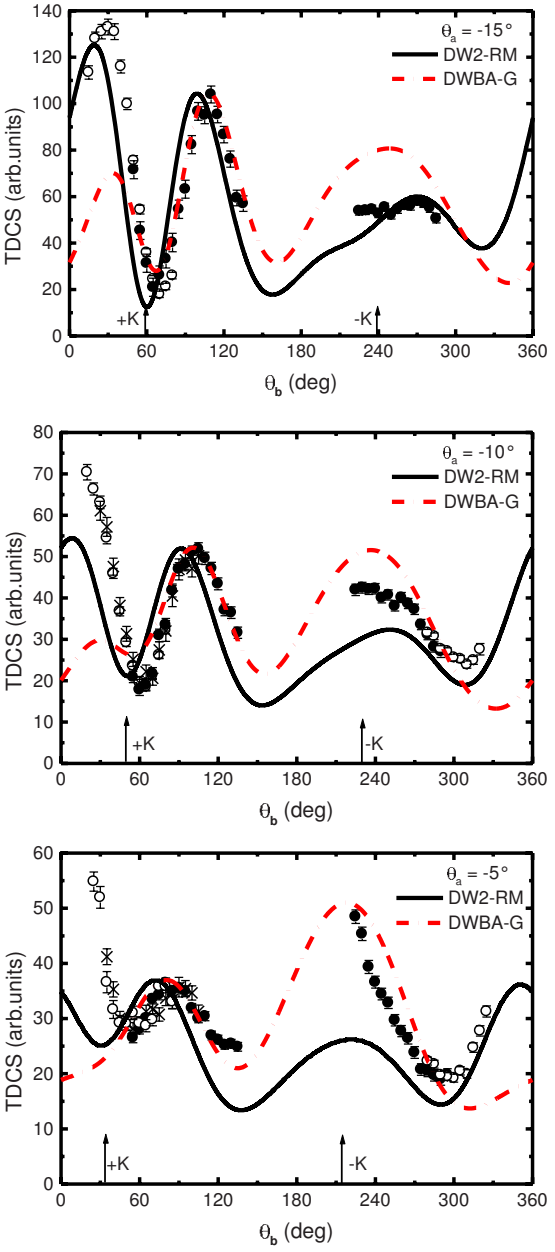

FIG. 4. (Color online) Measured and calculated triple differential cross sections for electron-impact ionization of the $2p$ orbital of neon, under kinematic conditions of $E_0=150$ eV and $E_b=10$ eV. Experimental results with the MAC turned on (open circles and crosses, corresponding to different deflections) and off (full circles) are shown. Both theoretical data sets have been normalized to the second lobe of the binary maxima.

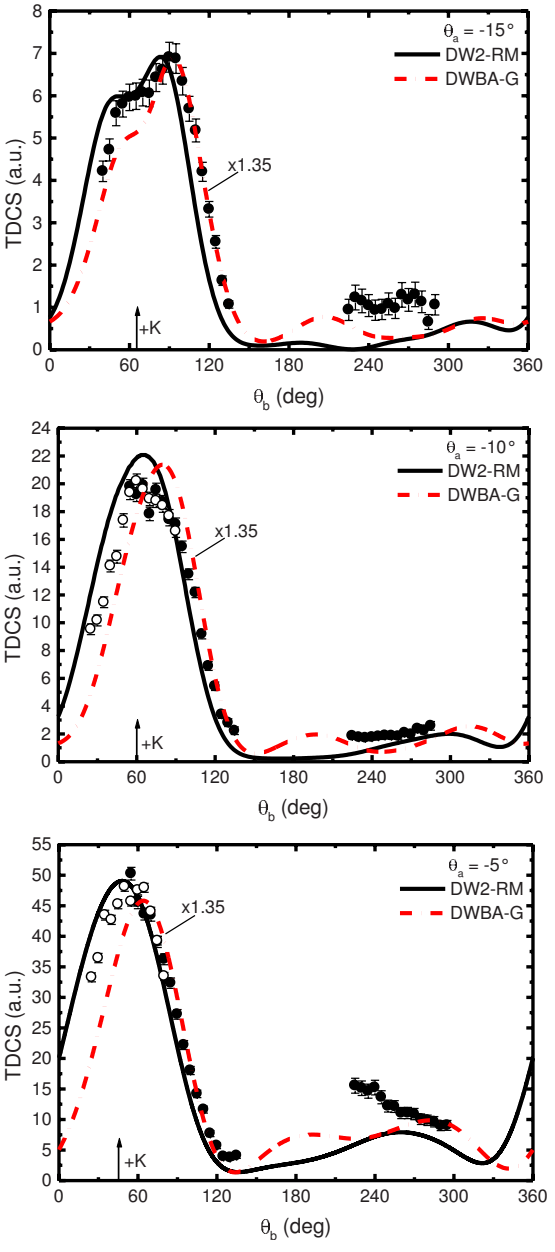

FIG. 5. (Color online) Measured and calculated triple differential cross sections for electron-impact ionization of the $5p$ orbital of xenon, under kinematic conditions of $E_0=150$ eV and $E_b=10$ eV. Experimental results with the MAC turned on (open circles) and off (full circles) are shown, with the experimental data normalized to the DW2-RM calculation at $\theta_a=-15°$.

both the shape of the cross section and the internormalized magnitudes. Although produced by very different methods, CCC and DWBA-G calculations give very similar results, with the CCC giving a larger recoil peak. These calculations essentially reproduce the binary peaks perfectly at $\theta_a=-15°$ and $\theta=-10°$, with the discrepancy in the internormalized magnitude at $\theta_a=-5°$ being within the internormalization uncertainty. The CCC also reproduces the magnitude of the recoil peak fairly well, with only a small angular shift present in some features. This could be considered as a surprising result given the relatively simple way in which the CCC models the target ionic core, and hence the ion-ejected electron interaction leading to recoil scattering. However, apart from the case at $\theta_a=-15°$, both the CCC and DWBA-G fail to reproduce the secondary recoil maximum, which is just apparent in the experimental data, and centered at $-\mathbf{K}$.

On the other hand, the DW2-RM calculation, with a more sophisticated treatment of the ion-ejected electron interaction via the R-matrix method, reproduces the magnitude and position of the second binary and both recoil peaks almost perfectly. This is at the expense of the binary to recoil ratio,

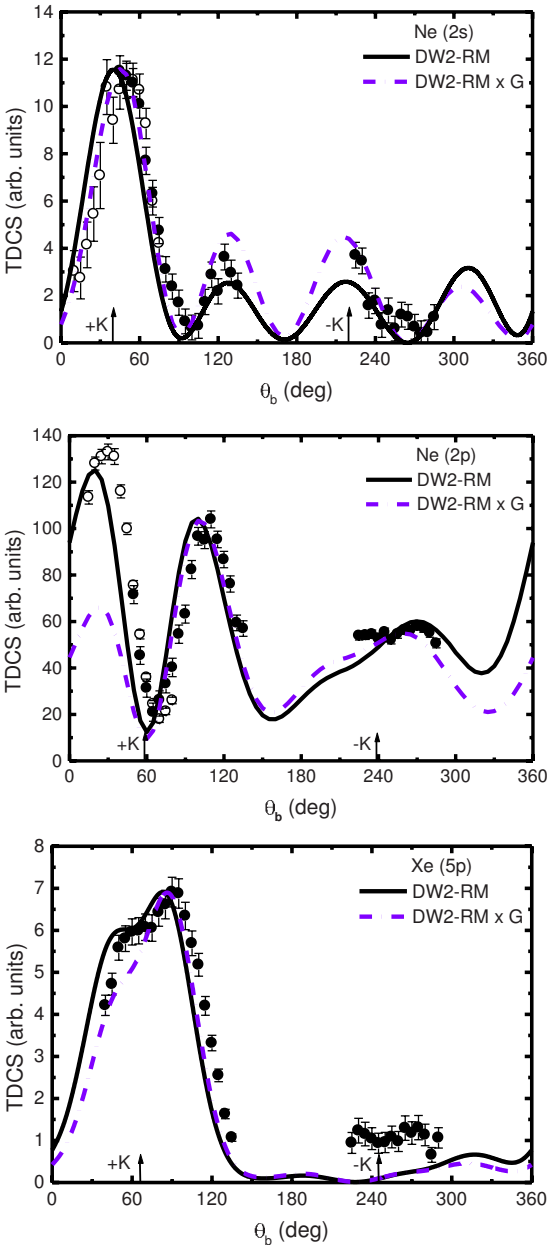

FIG. 6. (Color online) Measured and calculated triple differential cross sections for electron-impact ionization of several orbitals of neon and xenon, under kinematic conditions of $\theta_a=-15°$, $E_0=150$ eV, and $E_b=10$ eV. Experimental results with the MAC turned on (open circles) and off (full circles) are shown.

which is overestimated by increasing amounts as the scattering angle decreases. A shift of some 10°–20° is also present in the binary peak, again increasing as the scattering angle decreases. This can be attributed to the lack of PCI in the DW2-RM calculation, an effect that should become stronger as the scattering angle decreases and the ejected and scattered electrons emerge in closer proximity to each other. This assumption can be investigated by multiplying the DW2-RM by the Gamow factor to account approximately for PCI. The results of this procedure will be discussed further below.

Figure 3 presents a comparison between the experimentally internormalized neon $2p$ results and the theoretical calculations; in this case the experimental data at $\theta_a=-15°$ are normalized to the DW2-RM calculation at the second binary peak maximum. In this case, there is poorer agreement between the experimentally internormalized magnitudes and the predicted theoretical magnitudes than was the case for neon $2s$ ionization, with significant discrepancies being apparent for the $\theta_a=-5°$ case.

For ionization of the neon $2p$ orbital, the corresponding momentum transfers for $\theta_a=-15°$, $-10°$, and $-5°$ are 0.9, 0.66, and 0.46 a.u., respectively. For $\theta_a=-15°$, this corresponds to Bethe ridge kinematics, and the well-established trace of the p orbital momentum distribution can be seen, manifesting itself as a deep minimum in the binary peak near the momentum transfer direction. This trace is seen to weaken as the scattering angle decreases and the ion plays a more active role by recoiling to conserve momentum.

Given the discrepancies in the predicted magnitudes at the various scattering angles, it is difficult to make a shape comparison between the theoretically predicted cross sections and the measured data. Hence in Fig. 4 the theoretical results have been normalized to the second binary peak at all scattering angles, to enable a clearer shape comparison. At the scattering angle of −15°, the DW2-RM approach almost perfectly describes all measured features of the cross section, apart from an angular shift between the theory and experiment in the region of the first binary peak. This could be attributed to the fact that PCI is not included. The DWBA-G approach performs quite well but underestimates the magnitude of the first binary peak and overestimates that of the recoil peak. For the DWBA-G approach, a comparison with a DWBA calculation without the Gamow factor demonstrates that the reduced intensity in the first binary lobe and the decreased binary to recoil ratio can be attributed to multiplication by the Gamow factor. This strangely suggests that multiplying by the Gamow factor seems to worsen agreement for $2p$ ionization in the binary region, whereas it clearly improves agreement for $2s$ ionization.

As the scattering angle decreases, the DWBA-G approach shows improved agreement with the magnitude of the recoil peak, while the agreement in the recoil region between the DW2-RM method and the experimental data worsens. In the binary region, the discrepancies between theory and experiment warrant further analysis. The DWBA-G method predicts that the first binary peak should essentially vanish as the scattering angle decreases, a direct result of the behavior of the Gamow factor. The experimental data indicate that the second binary peak reduces relative to the first binary peak and the recoil peak; the first binary peak remains as a strong feature. The experimentally observed behavior of the first binary peak aligns more closely with the DW2-RM approach, which predicts that the first binary peak remains as the scattering angle decreases; however, this calculation does not include the effect of PCI. Intuitively, one might expect that structures in the cross section that fall in the region where the two electrons emerge in the same direction should be reduced in magnitude; the behavior of the first binary peak is hence unexpected (although it must be borne in mind that the two electrons emerge with quite different energies). As the data in this region are measured with the MAC, we have performed numerous tests to confirm the validity of the

data. As mentioned previously, test measurements with helium were performed immediately prior to the measurements on neon—only the target gas and the scattered electron energy were changed. In addition, for $\theta_a=-5°$ and $-10°$, multiple measurements were made with gradually increasing angular deflections of the ejected electron angular distribution; these different data sets are shown in Fig. 4, and demonstrate consistency in the behavior of the measured cross sections.

It is surprising that the DWBA-G method exhibits much superior agreement with experiment for the $2s$ orbital compared to the $2p$, as both orbitals are treated in the same manner in the DWBA calculation. What may be different is applicability of the Gamow factor, which is spherically symmetric, i.e., the s-wave component of the two-electron wave function describing PCI. The p symmetry of the target orbital might be somehow translated into the interelectron interaction, thus requiring higher partial waves to predict the effects of PCI successfully for p orbitals.

Although not possible at the moment, work is currently under way to extend the CCC calculation to p shells. The CCC method thus far has had great success in describing the physics of ionization of helium, including the three-body Coulomb interaction in the final state, and has proven successful for the neon $2s$ target in this and the previous study at a higher energy [8]. It will be most interesting to see how this calculation, which calculates the PCI in a completely different manner, predicts the behavior of the binary peak for ionization of a p orbital.

The results for ionization of the xenon $5p_{3/2}$ orbital are presented in Fig. 5. The experimental data are normalized in the binary region to the DW2-RM results at $\theta_a=-15°$, and the data at the other scattering angles are internormalized using the experimentally measured ratios. Here, the corresponding momentum transfers for $\theta_a=-15°$, $-10°$, and $-5°$ are 0.87, 0.61, and 0.38 a.u., respectively. As with the neon $2p$ case, the measurement at $\theta_a=-15°$ corresponds to Bethe ridge kinematics. However, for xenon only a weak trace of the p orbital momentum distribution is seen at this angle, and even this trace disappears at the smaller scattered electron angles. Also note that, again due to the different theories predicting different magnitudes for the cross section, the results from the DWBA calculation have been multiplied by a constant factor of 1.35 so that the magnitude of the binary peaks match at $\theta_a=-15°$.

The agreement between the measurements and theories in the binary region is generally good, with the DW2-RM approach describing the splitting of the binary peak slightly better at $\theta_a=-15°$. The magnitude of both calculations is generally consistent with the present experimental data at all scattered electron angles studied.

The recoil region of the cross section is much smaller than for neon $2p$ and exhibits very little structure. This region is reasonably well described by both calculations, with the exception that they appear to slightly underestimate the magnitude of the cross section in this region at all scattered electron angles. The experimental data also suggest a small recoil peak in the $-5°$ data, which is less pronounced in the theoretical results.

In order to further investigate the effect of the Gamow factor on the cross section for ionization of different orbitals, we have multiplied the DW2-RM results (for one scattering angle, $\theta_a=-15°$) by the Gamow factor; the results are presented in Fig. 6. For ionization of the $2s$ orbital in neon, this procedure brings the binary-recoil ratio into agreement with experiment, and partially accounts for the angular shift. However, for the case of ionization of the $2p$ orbital in neon and the $5p$ orbital in xenon, application of the Gamow factor significantly worsens agreement.

Application of the Gamow factor offers a mechanism for including the effects of postcollision interaction in the final channel approximately. An alternative treatment is to include the interaction directly in the final state wave function. In this approach (termed "3DW") [21], the incident, ejected and scattered electrons are described by distorted waves, and the Coulomb interaction is included in the description of the final state without approximation. It has been employed with some success to describe ionization of argon in the relevant energy regime (see, for example, [12,21]) and we are aware [22] that work is under way to apply this approach to the targets investigated here.

CONCLUSIONS

We have presented experimental and theoretical results for ionization of the valence orbitals of neon and xenon. The level of agreement between the various theoretical models and the experimental results illustrates that there is generally good agreement between the experiment and the various calculations for the case of ionization of the $2s$ orbital of neon and the $5p$ orbital of xenon, with the convergent close-coupling calculation performing particularly well in describing neon $2s$ ionization. The addition of the Gamow factor to a standard DWBA calculation also appears to produce very good agreement with experiment for ionization of these orbitals. The relatively small discrepancies between the DW2-RM calculation and experiment (particularly in relation to peak positions) could be attributed to the lack of inclusion of post collision interaction effects in the latter calculation. However, the situation in relation to ionization of the $2p$ orbital on neon is much less clear. There are major discrepancies between DWBA-G results and the experimental data at small angles; the DW2-RM approach is in somewhat better agreement with experiment, although the peak positions in the theoretical calculation diverge from those in the experimental data as the scattering angle decreases. However, application of the Gamow factor to the DW2-RM results undoubtedly worsens the agreement with experiment for this orbital. Further experimental and theoretical work is required to illuminate this situation.

ACKNOWLEDGMENTS

This work was supported by the Australian Research Council and the United States National Science Foundation Grant No. PHY-0757755.

[1] T. N. Rescigno, M. Baertschy, W. A. Issacs, and C. W. McCurdy, Science **286**, 2474 (1999).
[2] I. Bray, Phys. Rev. Lett. **89**, 273201 (2002).
[3] I. Bray and D. V. Fursa, Phys. Rev. A **54**, 2991 (1996).
[4] A. T. Stelbovics, I. Bray, D. V. Fursa, and K. Bartschat, Phys. Rev. A **71**, 052716 (2005).
[5] M. A. Haynes and B. Lohmann, J. Phys. B **33**, 4711 (2000).
[6] M. A. Haynes and B. Lohmann, Phys. Rev. A **64**, 044701 (2001).
[7] M. Stevenson, G. J. Leighton, A. Crowe, K. Bartschat, O. K. Vorov, and D. H. Madison, J. Phys. B **38**, 433 (2005).
[8] A. Naja, E. M. Staicu Casagrande, A. Lahmam-Bennani, M. Stevenson, B. Lohmann, C. Dal Cappello, K. Bartschat, A. Kheifets, and I. Bray, J. Phys. B **41**, 085205 (2008).
[9] A. Kheifets, A. Naja, E. M. Staicu Casagrande, and A. Lahmam-Bennani, J. Phys. B **41**, 145201 (2008).
[10] F. H. Read and J. M. Channing, Rev. Sci. Instrum. **67**, 2372 (1996).
[11] M. A. Stevenson and B. Lohmann, Phys. Rev. A **73**, 020701(R) (2006).
[12] M. A. Stevenson and B. Lohmann, Phys. Rev. A **77**, 032708 (2008).
[13] K. Bartschat and P. G. Burke, J. Phys. B **20**, 3191 (1987).
[14] K. Bartschat, Comput. Phys. Commun. **75**, 219 (1993).
[15] R. H. G. Reid, K. Bartschat, and A. Raeker, J. Phys. B **31**, 563 (1998); **33**, 5261(E) (2000).
[16] P. G. Burke and K. T. Taylor, J. Phys. B **8**, 2620 (1975).
[17] L. V. Chernysheva, N. A. Cherepkov, and V. Radojevic, Comput. Phys. Commun. **18**, 87 (1979).
[18] M. Brauner, J. S. Briggs, H. Klar, J. T. Broad, T. Rosel, K. Jung., and H. Ehrhardt, J. Phys. B **24**, 657 (1991).
[19] M. Dürr, C. Dimopoulou, B. Najjari, A. Dorn, and J. Ullrich, Phys. Rev. Lett. **96**, 243202 (2006).
[20] M. Inokuti, Rev. Mod. Phys. **43**, 297 (1971).
[21] A. Prideaux, D. H. Madison, and K. Bartschat, Phys. Rev. A **72**, 032702 (2005).
[22] D. H. Madison (private communication).